Methodological Considerations in Cover-Collapse Sinkhole Analyses: A Case Study of Southeastern China's Guangzhou City

Long Jia[a,b,c], Yan Meng[a,b,c], Lujuan Li[b], Renchao Yin[b,c],
[a]China University of Geosciences, Wuhan 430074,China
[b]Institute of Karst Geology, Chinese Academy of Geological Sciences, Guilin 541004, China
[c]Key Laboratory of Karst Collapse Prevention, CAGS, Guilin 541004, China

Abstract

Cover-collapse sinkholes can present significant hazards to ~~human habitation and communal facilities~~ in soil-covered karst regions. Therefore, for human security and land-use planning in sinkhole-prone areas, appropriate approaches are required prior to construction in order to understand the cover-collapse sinkhole genesis and its likely evolution. The study seeks to contribute to performing an integrated analysis of karst hazards in mantle karst regions where karst evidence can be masked, with the ultimate goal of developing a methodological framework utilizing different techniques and approaches. A small area located in Guangzhou City of southeastern China's Guangdong Province was analyzed. The detailed typology, morphometry, and chronology inventory of 49 cover-collapse sinkholes in the study area were analyzed using various surface investigation methods, such as field surveys, aerial photography, and photogrammetry. The Quaternary deposits and indicators of the active underground karst features in the aforementioned mantle karst region were geotechnically characterized using drilling and geophysical techniques. These techniques included ground penetrating radar (GPR), electrical resistivity imaging (ERI), natural source audio frequency magnetotellurics (NSAMT), and micro-tremors. During ~~this study's~~ investigations, three karst fissure zones covered by Quaternary soil were ~~observed~~ using multiple techniques. In addition, it was found that the groundwater dynamic monitoring data confirmed that the sinkholes in the study area were closely related to changes in groundwater levels. Therefore, the efforts which have been made to investigate and monitor the sinkhole development will be required to continue

into the immediate future.

Keywords: cover-collapse sinkholes; karst; geomorphological analyses; geophysical surveys

1. Introduction

As near-surface indicators of active karst features in soil-covered karst regions, cover-collapse sinkholes are the result of the downward water-borne transportation of soil or other related material into underlying voids in either limestone bedrock or other soil profiles. Cover-collapse sinkholes are characterized by roughly circular outlines, internal drainage, and distinct breaks in the land surface *(Tharp, 1999, 2002)*. Cover-collapse sinkholes are known to occur in many regions of the world *(Galve et al., 2015; Zhou and Lei, 2017)*, and have caused serious damages to urban and industrial areas, as well as farming regions. Therefore, due to the large and increasing impacts of sinkhole damages, including the loss of human lives, various techniques and approaches focusing on the reconstruction of cover-collapse sinkhole conditions have received increasing attention *(Kaufmann et al., 2018; Pueyo Anchuela et al., 2015; Zini et al., 2015)*. These techniques and approaches can be divided into the following categories:

(1) ***Field and photogrammetric surveys***: These surveys include historical satellite remote sensing images, aerial photograph interpretations, and field surveys, which are often useful to analyze the morphometry and chronology of cover-collapse sinkholes *(Al-Halbouni et al., 2017; Gutiérrez et al., 2007)*;.

(2) ***Non-invasive geophysical techniques***:

Subsurface cavities and the processes that lead to the development of sinkholes cause changes within the subsurface, such as porosity, fracture density, and water saturation *(Frumkin et al., 2011)*. Before collapse, non-invasive geophysical approaches may detect these changes, and include various techniques such as microgravity *(Debeglia et al., 2006; Eppelbaum et al., 2008; Paine et al., 2012)*; micro-tremors

(Maresca and Berrino, 2016); electrical resistivity tomography ***(Ahmed and Carpenter, 2003; Gutiérrez et al., 2019)***; seismic reflections ***(Wadas et al., 2017)***; and electromagnetic surveys including GPR ***(Ronen et al., 2019).***

(3) ***Invasive techniques***: Invasive techniques include trenching ***(Gutiérrez et al., 2009)***; drilling ***(Cueto et al., 2018)***; and geophysical well logging. Trenching and drilling processes are able to provide immediate information on the nature and geotechnical properties of underground areas. Geophysical well logging can contribute to filling the significant gaps which drilling processes and non-invasive geophysical methods are unable to address.

(4) ***Monitoring***: Hydrogeological monitoring ***(Jiang et al., 2019)*** and ground deformation monitoring ***(Galve et al., 2015)*** are commonly crucial aspects for understanding the causes of deformations, and are adopted to assess and predict the kinematics of the subsidence phenomena. In particular, these monitoring methods are necessary in cases of potential episodes of catastrophic collapse.

Karstic terrain is one of the most difficult natural geological hazards to assess for development and construction unless proper measures are taken ***(Xeidakis et al., 2004)***. Due to the high vertical and lateral variabilities of the geological and hydrogeological characteristics in ~~the~~ karst ~~regions~~, no single technique ~~has been found which~~ can effectively resolve the related problems. Therefore, in the present study, a small ~~rigion~~ with surface deformation issues located in southeastern China's Guangzhou City was examined for the purpose of developing a methodological framework for the evaluations of the potential conditioning factors which control the occurrences of sinkholes in soil-covered ~~karst regions~~ where karst evidence may be hidden.

2. Geological setting

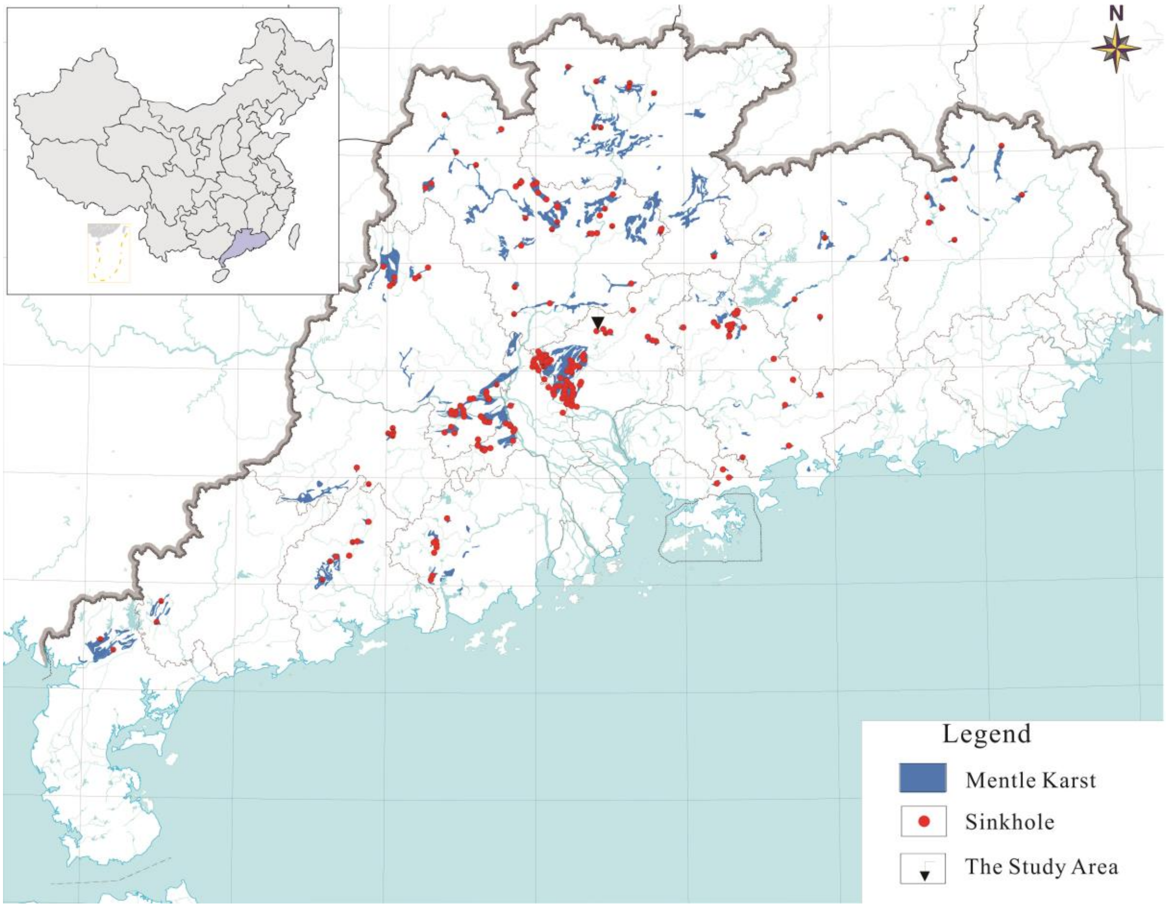

Figure 1. Karst sinkhole (affecting more than 100 people) distributions in China's Guangdong Province

From a geographical perspective, the study area ~~was~~ located in the central sector of the Pearl River Delta, in Conghua District of Guangzhou City, Guangdong Province, ~~in the~~ southeastern ~~region of~~ China. ~~The geologic hazards related to cover~~-collapse sinkholes have occurred frequently in China's Guangdong Province in recent years. As shown in Fig. 1, according to the statistical data, there were more than 400 large-scale karst cover-collapse sinkholes (affecting more than 100 people) in Guangdong Province.

The elevations in the study area ~~had varied~~ between 30 and 80 m above sea level~~, as shown in Fig. 2~~. Quaternary deposits ~~were observed to~~ mantle the vast majority of the Carboniferous limestone. ~~These consisted~~ of alluvial deposits with thick layers (4.65 to 13.8 m) of loose soil (China Geological Map, F-49-24-A Conghua, Scale 1:50.000). The karst processes in the region were determined to be related to the dissolution of Miocene ~~Carbonate material,~~ mainly covered by Quaternary material. In addition, Jurassic volcanic strata and carboniferous sandstone strata ~~were~~ also ~~distributed in the study area~~. The evolution processes of the sinkholes appeared to be structurally controlled by the ~~characteristics of the~~ local and regional faulting. The most important tectonic feature in the area ~~was~~ the “Guangzhou-Conghua” fracture (~~which was~~ buried within the study area ~~and recognizable only inpart~~) with a ~~typically~~ 60 ° NW orientation. ~~Generally speaking, a~~ large part of the investigated area ~~was~~ occupied by paddy fields, and buildings ~~were~~ relatively scarce. The cover-collapse sinkholes ~~were~~ evidenced in the alluvial plane of the study area.

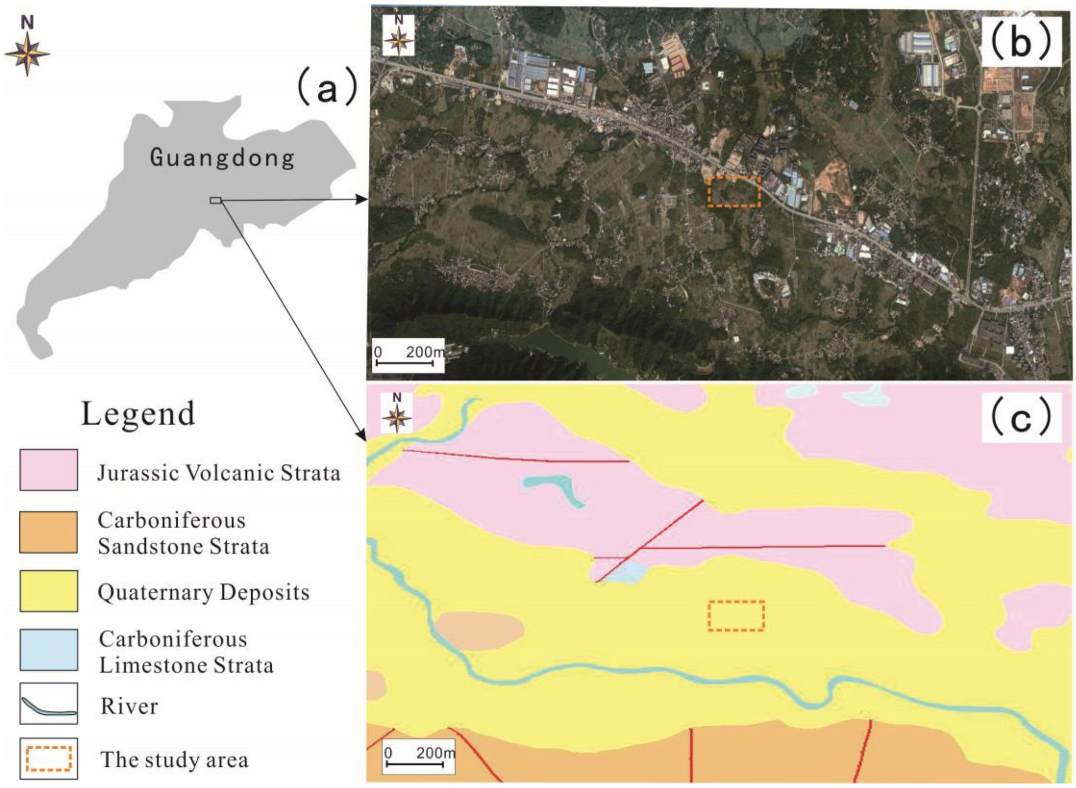

Figure 2. Geological and geomorphological setting of the study area: (a) Location of the study area in Guangdong Province of southeastern China; (b) ©Google Earth image showing the study sites. The study sites as mapped by the authors are shown (red rectangle); (c) Synthetic exposed stratigraphic map

3. Methodology

In order to understand the causes of the deformations, including sudden catastrophic collapses, as well as accurately predict the kinematics of the subsidence phenomena in the study area, multidisciplinary approaches were planned for the following purposes: 1. To ascertain the surface subsidence and sinkhole features; 2. To precisely locate and define the subsurface karst features at depth, such as cavities, conduits, and karst fissure zones; 3. To detect the thicknesses and ~~stratification~~ of soil and underlying subsidence features; and 4. To monitor groundwater dynamic ~~conditions and deformations~~.

3.1 Surface investigations

3.1.1 Field survey, documentary information and oral information

During the initial phase of this study's investigation, information data related to the selected sinkhole areas which had been obtained from written documents, such as local maps or reports from public institutions, were collected and analyzed in order to gain a good understanding of cover-collapse sinkhole context. For example, previous cartographic production data were utilized, such as a local 1:50,000 scale geological map. Also, the available rough information regarding the alluvium thickness, ground elevations, and ~~formation~~ lithology were used in this study. During the investigation process, detailed field surveys annotating 1:1000 scale color telephotographs were carried out in the selected sinkhole areas. In addition, information from local residents was found to substantially enrich the investigation content by providing data on the spatial and temporal distributions of undetected and filled sinkholes, along with the weather conditions and well water level changes at that time.

3.1.2 Aerial photogrammetry and historical satellite remote sensing images

In aerial photogrammetry, unmanned aerial vehicle (UAV) platforms can be used to capture digital surface and terrain models for large scale mapping, with an accuracy down to the cm-level from various waypoints in investigated regions ***(Chiabrando et al., 2011; Lee et al., 2016; Yeh et al., 2016)***. In the present study, detailed and accurate geomorphological data including surface elevation of the study area were provided by senseFly mapping drones using Postflight Terra 3D software. Also, historical images available from Google Earth were used to obtain information on the recent morphological changes of the ~~analyzed~~ sinkholes in the study area. The detailed interpretations of photographs taken on different dates (2014/10/28; 2015/12/05) assisted in this study's analysis of the spatio-temporal distribution patterns of the subsidence phenomena.

3.2 Non-intrusive geophysical prospecting

3.2.1 Surface-based GPR

Ground Penetrating Radar (GPR) surveys are a type of geophysical technique which offer a very high resolution abilities in order to locate and characterize the sedimentological information of subsoil (such as soil-cavities and the presence of active subsidence, and so on) *(Anchuela et al., 2009; Chalikakis et al., 2011; Lei et al., 2008)*. In GPR profiles, information can be identified by changes in color, which are related to the amplitude of the recorded wave at each point. However, this technique has been found to have its own shortcomings, due to the fact that the depths of surface-based GPR detections were generally found to be only 3 to 5 m in southern China. In the present study, 20 surface-based GPR ~~(Ground Penetrating Radar)~~ profiles with a total length of 3 km were conducted in the study area, as detailed in Fig. 2. The continuous GPR profiles were collected utilizing a SIR3000 GPR instrument manufactured by the Geophysical Survey System Inc. (GSSI) in the United States, ~~equiped~~ with a 100 MHz bowtie bistatic antenna.

3.2.2 Micro-tremors

Micro-tremors are passive source vibration signals which originate from natural or human activities. These vibration signals carry abundant information regarding underground geological structures. The Nakamura technique of microtremor exploration, also known as the H/V ratio method, is a widely used passive seismic technique by researchers for obtaining overburden sedimentary layer thicknesses *(Dinesh et al., 2010)*. With this technique, the calibration relationships between the soil thicknesses and the prominent resonant frequencies in the H/V spectrum are obtained from borehole drilling logs. Therefore, the resonant frequencies can be used to obtain the thicknesses of the sediment in the area near the borehole. In this study, single-station micro-tremor data came from a Tromino 3G seismograph were collected from the 318 sites. The sites were spaced 5 m apart, and the single point collection time was 20 minutes.

3.2.3 Electrical resistivity imaging (ERI)

Electrical resistivity imaging (ERI) is a technique in which many individual resistivity measurements are combined to produce a resistivity cross-section of the subsurface. Electrical parameters, such as resistivity or conductivity, are very sensitive to formation properties. Therefore, ERI methods have been effectively used for differentiation processes related to rock layers. Electrical resistivity tomography profiling (surface electrode arrays) is also commonly used for sinkhole investigations as a means of identifying shallow limestone deposits, large dissolution feature zones, and underlying cavities ***(Fabregat et al., 2017)***. In the present study, two ERI (electrical resistivity image) profiles, with a total length of 500 m and spacing of 30 m, were conducted in the study area. The resistivity lines of this pattern were acquired utilizing a WDJD-3 Superstring multi-channel and multi-electrode resistivity system designed in China, equipped with 60 electrodes spaced at 5 m intervals along each line. The data were inverted using RES2DINV software.

3.2.4 Natural source audio frequency magnetotellurics (NSAMT)

Audio frequency magnetotelluric (AMT) methods involve surface-based electromagnetic sounding techniques which use fixed grounde~~d~~ dipoles as signal sources (CSAMT), or alternatively, the naturally-occurring fields of the Earth’s atmospheric system (NSAMT). The higher frequency audio-magnetotelluric (AMT) methods are able to detect the ranges of karst fissure zones based on the different electrical conductivity of the underground rock strata. Once water flows into caved and fractured zones, the resistivity of those areas will rapidly decrease. These are referred to as low-resistivity anomaly zones. In this study, the naturally-occurring electromagnetic fields were used as the signal sources. Then, NSAMT (Natural Source Audio Frequency Magnetotelluric) profiles with total lengths of 500 m were conducted in the areas coinciding with the ERI profiles. The NSAMT data were collected using a

Geometrics StrataGem EH4 system in the study area. Then, an EH-4 conductivity imaging system manufactured by EMI and Geometrics (US), was adopted in this study as the electromagnetic geophysical detection system for the auto data acquisition and processing procedures.

3.3 Intrusive techniques

3.3.1 Drilling

Drilling processes provide valuable information on the nature and geotechnical properties of underground areas and assists in the recognition of voids (including soil caves, karst caves, and karst conduits) and sediment (disturbed by subsidence processes). Six boreholes were arranged in a selected sector of Bumei Village, with a total ~~footage~~ of 407 m, which were referred to as the drilled cores.

3.3.2 Single-hole radar

Single-hole radar techniques are commonly utilized to record single-hole full-waveform radar data. These data can potentially supply information on the nature of the reflectors distributed along the boreholes ***(Kim et al., 2007)***. A fixed-offset transmitter- and receiver-antennae pair were pulled slowly up the length of a borehole during the single-hole radar detection process. The principle of the single-hole reflection method is similar to that of surface-based GPR, with the exception that reflectors may occur on all sides of the borehole recording line. Planar features, such as fault surfaces, which may be intersected by a borehole, will appear as V-shaped reflections in a single-hole radar section. The images of the point reflectors (for example, karst caves) are hyperbola. In the current study, a MALA system equipped with 100 MHz borehole antennae was used to acquire all of the radar data. The single-hole full-waveform data were recorded in all six holes utilizing transmitter and receiver antennae separated by 2.75 m.

3.3.3 Cross-hole radar

Cross-hole GPR is a trans-illumination survey method in which two antennae are lowered down into adjacent parallel boreholes ***(Bachrach et al., 2005; Cordua et al., 2009)***. Then, by transmitting radar signals from one borehole to another, the electromagnetic EM wave velocity and attenuation between the two boreholes can be estimated. The high-resolution imaging of subsurface electromagnetic EM wave velocities has proven to be effective in detections conducted in the majority of water-filled areas, such as water-filled faults and caves, in which the low-speed zones represent the water filled areas ***(Tan et al., 2012)***. In this study, three pairs of boreholes were used for cross-hole radar surveys, taking advantage of the adopted MALA system with 100 MHz borehole antennae.

3.4 Monitoring methodologies

3.4.1 Hydro-dynamic monitoring

In many parts of the world (including China), recent research reports have revealed that a major proportion of recent cover-collapse sinkhole events have been induced by anthropogenic changes in hydrogeological systems ***(Anikeev, 1999; Lei et al., 2016; Meng et al., 2014)***. Therefore, the monitoring of groundwater levels may become an effective method for capturing real-time changes in the underground hydrodynamic forces, and possibly even used to forecast the ~~appearances~~ of cover-collapse sinkholes. In the study area, the water levels in two of the boreholes had been monitored since January of 2015. The monitoring intervals were 20 minutes.

3.4.2 InSAR

Interferometric Synthetic Aperture Radar (InSAR) analysis methods can be used to screen large areas for anomalous vertical movements, as well as to guide intensive field investigations and detection processes to areas where significant changes are occurring ***(Intrieri et al., 2015)***. In addition, the mapping of ground displacements may assist in the identification of locations prone to future cover-collapse sinkholes. In the study area, InSAR ground deformation data were obtained with a 5 m pixel size and a vertical accuracy higher than 3 m. Then, three RADARSAT-2 Ultra Fine images from November 27^{th} of 2015, January 14^{th} of 2016, and March 2^{nd} of 2016 were selected for further examination.

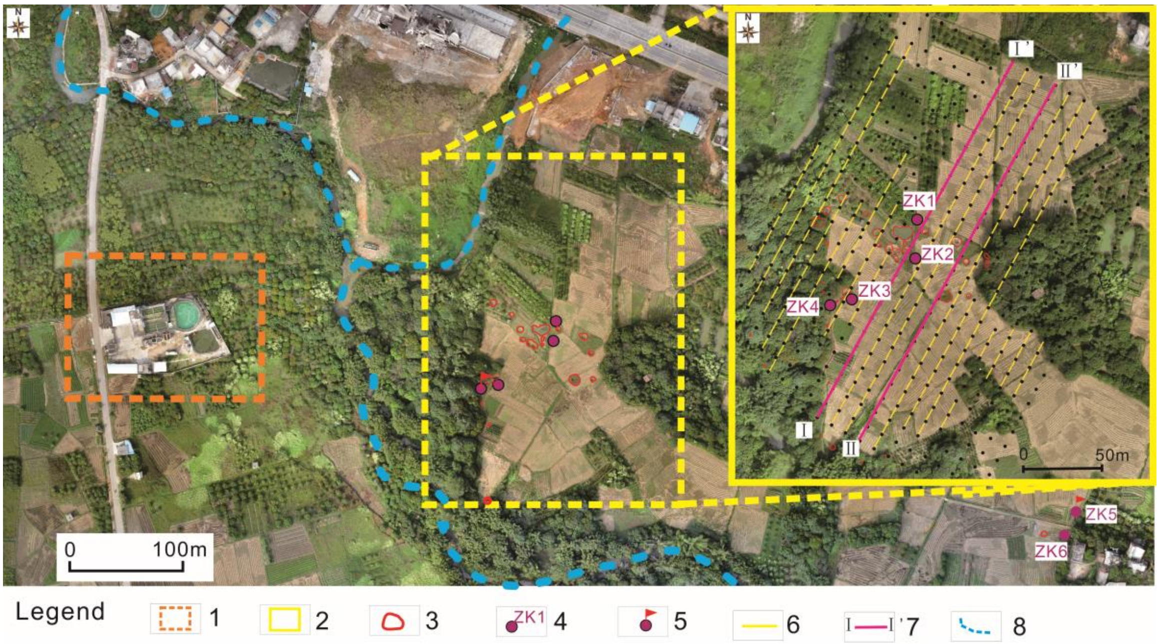

Figure 3. Investigation layout of the research area (Background image from aerial photograph provided by the authors' senseFly mapping drone): 1. Waterworks; 2. Research areas; 3. Sinkhole pits; 4. Boreholes; 5. Groundwater level monitoring points; 6. Ground penetrating radar lines; 7. Geophysical detection lines (GPR, ERI, and AMT); 8. Brook area

4. Results

4.1 Sinkhole inventory

The field surveys with drones aerial photogrammetry, along with the historical satellite remote sensing images, ~~had~~ assisted in ~~the~~ mapping ~~of~~ the sinkhole ~~detailed inventory to be accomplished~~, as shown in ~~Fig. 3, Fig. 4b and Fig. 5a~~. There were 49 cover-collapse sinkholes observed in the selected area. Table 1 presents the morphometry and chronology of the inventoried sinkholes. These collapses, which ~~had~~ resulted in direct economic losses, ~~had~~ mainly occurred between September ~~of~~ 2014 and March ~~of~~ 2015. The Google Earth images ~~from prior to~~ 2014 showed no sinkholes in the area. In addition, 47 collapse pits were identified in the aerial photographs from 2014 to 2015. Two more sinkholes had formed in the area in October ~~of~~ 2016 and March ~~of~~ 2017, respectively. No casualties ~~had~~ resulted from the sinkhole collapses. However, a portion of the rice harvest was lost and some of the fruit trees in the area were destroyed.

Table 1 The dimensions and dates of sinkholes

ID	Shape	Diameter or Major axis/ Minor axis	Major axis direction	Date and time	Depth	ID	Shape	Diameter or Major axis/ Minor axis	Major axis directi on	Date and time	Depth
1	Circle	2.8		Sep-14	0.9	25	Ellipse	0.9/0.6	0	Sep-14	0.5
2	Circle	7.8		Sep-14	0.8	26	Circle	1.7		Sep-14	1
3	Circle	3.1		Jun-14	0.9	27	Ellipse	1.8/0.9	120	Sep-14	1
4	Circle	4.9		Sep-14	1	28	Circle	3.3		Sep-14	1
5	Circle	3.2		Sep-14	1	29	Ellipse	1.3/1		Sep-14	0.98
6	Ellipse	13.4/7.2		Sep-14	1.2	30	Ellipse	2.2/1.5	205	Oct-14	1
7	Circle	2.6		Sep-14	2	31	Circle	2.6/1.8	345	Oct-14	0.9
8	Circle	3.2		Sep-14	1.5	32	Circle	1		Sep-14	1
9	Circle	4.5		Sep-14	0.8	33	Ellipse	2.1/1.3	280	Jan-15	1.5
10	Circle	4.8		Sep-14	0.9	34	Ellipse	3.7		Dec-14	2
11	Circle	1.8		Sep-14	0.8	35	Ellipse	8/6		Sep-14	1
12	Circle	2.4		Sep-14	0.9	36	Ellipse	12/6		Nov-14	2.2
13	Circle	2.3		Sep-14	1	37	Circle	1.8		Nov-14	0.4
14	Circle	4.0		Sep-14	0.8	38	Ellipse	2.8/1.2	40	Mar-15	1
15	Circle	3.2		Sep-14	1.5	39	Circle	1.9		Mar-15	1.35
16	Circle	1.8		Sep-14	1.5	40	Circle	1.8		Nov-14	0.7
17	Ellipse	4.6/3.8	290	Sep-14	1.3	41	Circle	1.7		Nov-14	0.7
18	Circle	2.1		Sep-14	0.75	42	Circle	2.4		Nov-14	1.1
19	Ellipse	2.4/2	85	Sep-14	0.7	43	Ellipse	1.3/0.5	0	Nov-14	0.7
20	Ellipse	2.2/1.9	45	Sep-14	0.38	44	Ellipse	1.2/0.8	10	Nov-14	2
21	Ellipse	2/1.2	115	Sep-14	1.5	45	Circle	1.1/0.5	10	Nov-14	0.2
22	Circle	1.6		Sep-14	1.6	46	Circle	1.5		Nov-14	0.5
23	Ellipse	9.5/7.0	280	Sep-14	2	47	Circle	8.5		Nov-14	1.4
24	Ellipse	13/7	7	Sep-14	2	48	Circle	2.1		Oct-14	0.8
						49	Circle	2		Nov-16	0.9

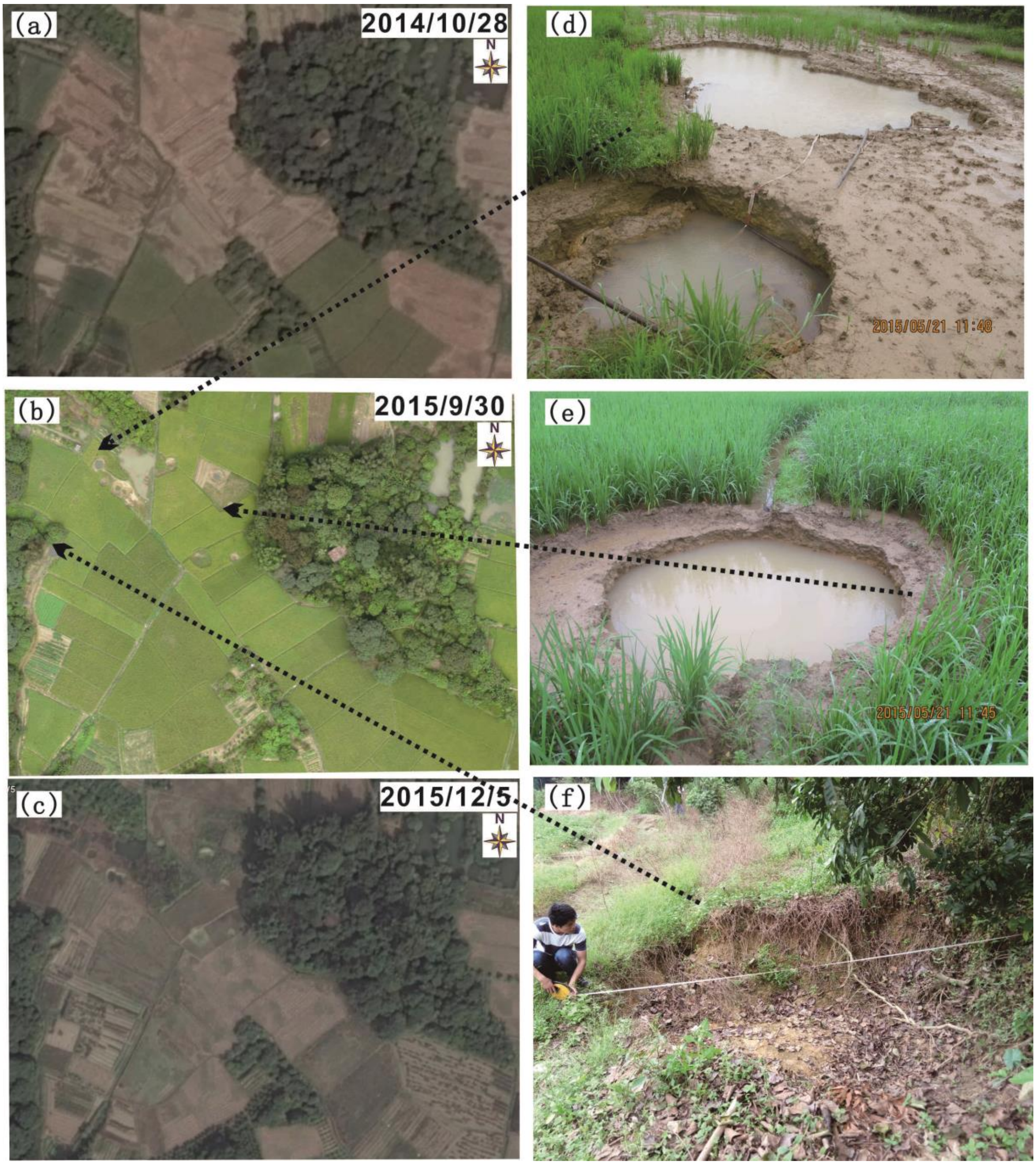

Figure 4. Sinkhole images in the research area: (a) and (c) ©Google Earth image showing the study site on October 28, 2014 and December 5, 2015; (b) Aerial photograph provided by the authors' senseFly mapping drone on September 30, 2015; (d), (e), and (f) Sinkhole camera photos

4.2 Soil layers

The thicknesses and structures of the soil layers in the study area were ~~obtained according to the results of the~~ drilling, micro-tremors, and electrical resistivity imaging (ERI).

4.2.1 Quaternary soil thicknesses

The drilling profiles showed that the thicknesses of the ~~quaternary~~ soil layers in the collapsed intensive area ranged between 9 and 14.2 m in Fig. 7. In order to obtain a comprehensive understanding of the Quaternary soil thicknesses in the study area, a contour map of the buried depths of the ground bedrock was obtained by utilizing a micro-motion inversion method ~~in Fig. 5b~~. In the southwestern area of the site, the bedrock was determined to be between 12 and 15 m in depth. In the other areas of the site, the thicknesses of the soil layers averaged approximately 10 m. The majority of the collapses had occurred in the areas where the depths of bedrock had varied greatly.

4.2.2 Quaternary soil structure

The borehole dates had revealed that the structures of the soil layers changed greatly, as detailed in Fig. 7. As determined from the drilling profiles, from the bottom to the top in the figure, the stratigraphy of the area was characterized by the following: (1) Paleozoic carboniferous Shitengzi formations (C_1s, limestone); (2) Quaternary alluvial layers (Qal, sand) or residual soil layers (Qel, clay); and (3) Planting soil layers (Qpd). The two obtained ERI profiles in Fig. 6b and 6e revealed a high resistivity zone in the southern surface of the study area. In addition, when combined with the results of this study's field investigations, it was confirmed that there was a high resistance zone in Quaternary alluvial layers (Qal, sand). There was also a low resistivity zone in Fig. 6b and 6e ~~indentified~~ on the northern surface of the study area, which represented the Quaternary residual soil layers (Qel, clay) distribution area.

4.3 Karst features

Karst caves were discovered in four out of a total of 6 boreholes, and were considered to be the most direct evidence of karst activities in the study ara. In addition, other karst caves and fissures around the boreholes were discovered using geological borehole radar. It was found that, based on the transmission time imaging of the cross-hole radar, a karst cave ~~with an elevation of between~~ 3 and 9 m existed between ~~drilling~~ boreholes ZK1 and ZK2. Also, between ~~drilling~~ boreholes ZK5 and ZK6, the radar signal low-speed zones represented water-filled karst caves and fissures in Fig. 7. Furthermore, the results of the single-hole radar measurements showed that there were linear anomalies located around boreholes ZK1, ZK5 and ZK6, indicating the existence of karst cracks in those areas.

As ~~indiated~~ in L1, L2 and L3 of Fig. 6, three low-resistivity anomaly zones revealed fault zone structures in the overburden karst area ~~sites,~~ as identified in the ERI and EH4 profiles. The micro-tremor detection data showed that the bedrock surfaces fluctuated greatly in the southwestern section of the study area in Fig. 5. These findings were found to be consistent with the abnormal positions revealed in the ERI and EH4 profiles. Furthermore, these results ~~had~~ indicated the specific locations and morphology of the karst fracture zones.

In the present investigation, no soil caves were found in the survey line by surface-based GPR in Figs. 6a and 6d, which was consistent with the fact that no collapses had occurred in the survey area. The disturbed and loose areas in the Quaternary overburden were delineated by surface-based GPR at a position of 70 to 120 m in profile Ⅰ-Ⅰ' and at 40 to 100 m in profile Ⅱ-Ⅱ', excluding the disturbance data.

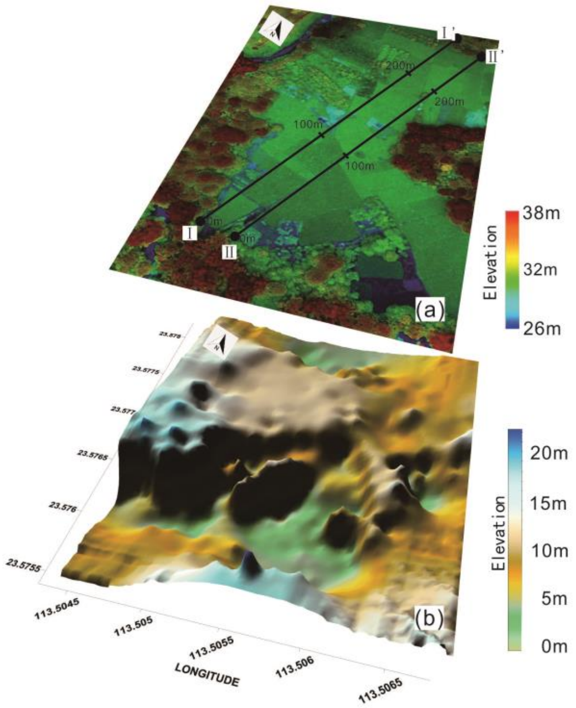

Figure 5. Geomorphological map and bedrock elevation map: (a) geomorphological map including surface elevation from the authors' senseFly mapping drone; (b) Bedrock elevation map was obtained by utilizing a micro-motion inversion method. Ⅰ-Ⅰ', Ⅱ-Ⅱ': Geophysical profile line

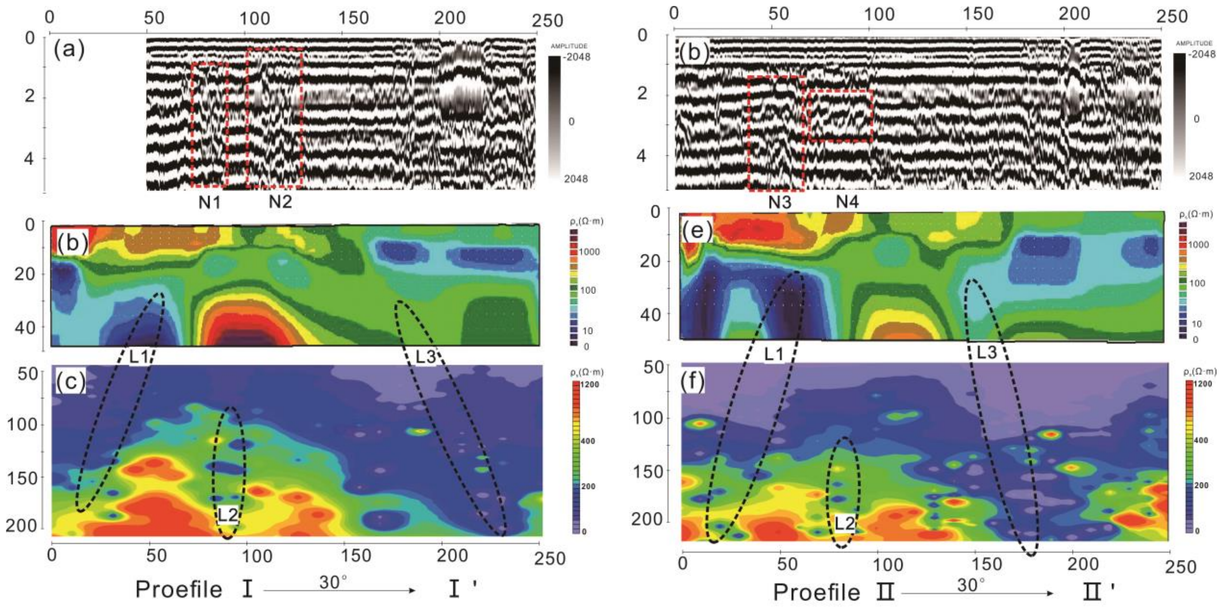

Figure 6. Geophysical interpretations of profiles: (a) Interpreted GPR section of profile Ⅰ-Ⅰ'; (b) Interpreted ERI section of profile Ⅰ-Ⅰ'; (c) Interpreted NSAMT section of profile Ⅰ-Ⅰ'; (d) Interpreted GPR section of profile Ⅱ-Ⅱ'; (e) Interpreted ERI section of profile Ⅱ-Ⅱ'; (f) Interpreted NSAMT section of profile Ⅱ-Ⅱ'; L1, L2, and L3 revealing the low-resistivity anomaly zones; N1 to N4 refer to the disturbed and loose zones, respectively

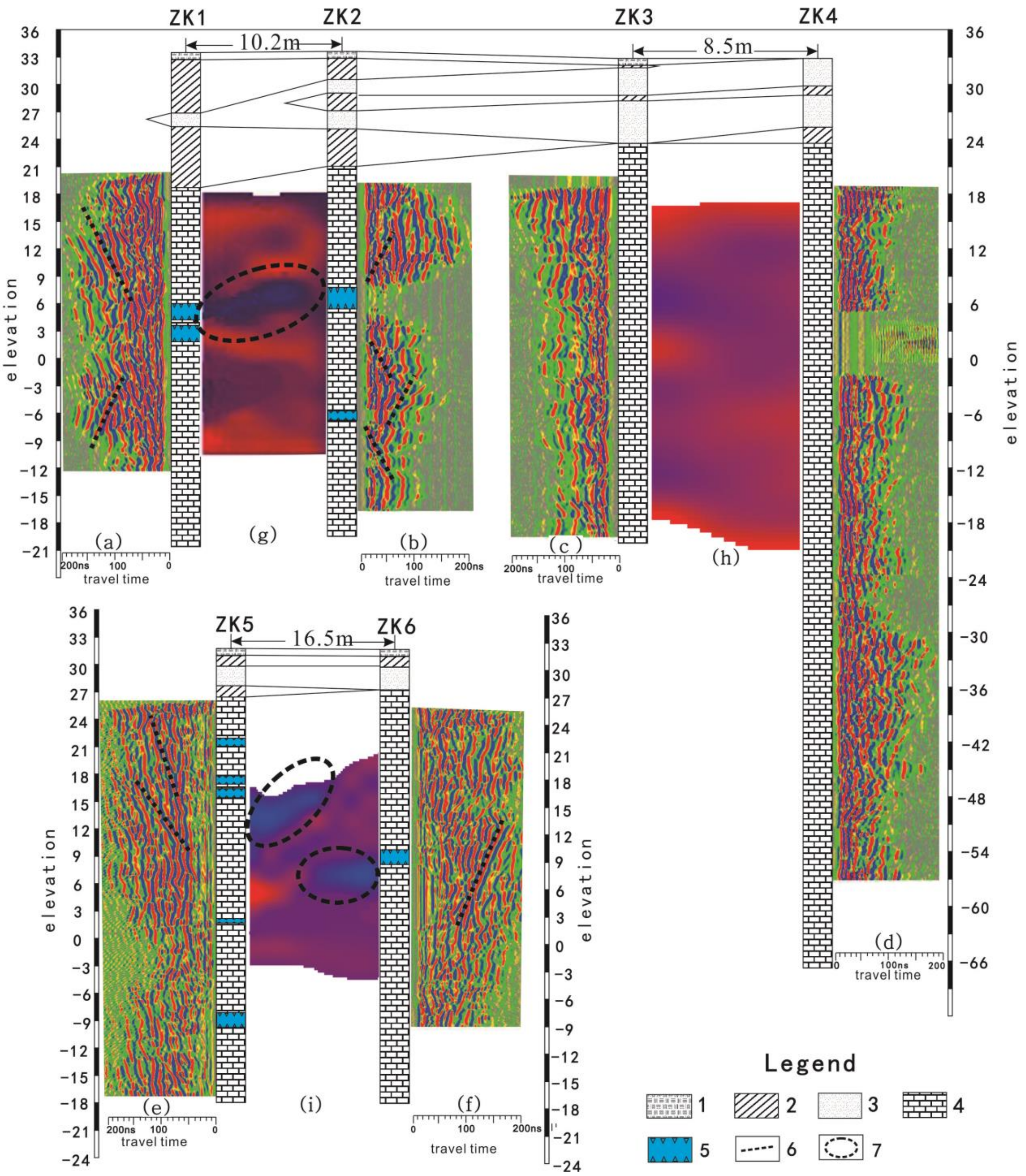

Figure 7. Borehole histogram and borehole radar images. (a) to (f) show the single-hole radar reflection images in which ZK1 to ZK6 show the borehole histogram; (g) to (i) are the cross-hole radar transillumination images: 1. Planting soil layers; 2. Quaternary residual soil layers (clay); 3. Quaternary alluvial soil layers (sand); 4. Paleozoic Carboniferous limestone; 5. Karst cave; 6. Karst fissures; 7. Low-speed zones representing the water filled areas

4.4 Changes in groundwater levels

In accordance with the information obtained from the local residents and staff, the daily water output of a waterworks located 800 m east of the study area was approximately 1,200 to 6,000 m^3. The change of water output was related to the water consumption of the residents. the water levels of the local wells had dropped by about 7 m in early 2015 when a large scale karst collapse had occurred in the study area. Also, on the basis of the hydrodynamic monitoring data, it was confirmed that there was a relationship between groundwater level changes and the aforementioned collapse in the study area, as shown in Fig. 8. In additon, the water table in the study area had experienced an approximate 8 m drop during the period ~~ranging~~ from October ~~of~~ 2016 to December ~~of~~ 2017. It ~~had been~~ recorded that during this same period, two new cover-collapse sinkholes had formed. However, since August ~~of~~ 2018, the groundwater levels have recovered, and no further karst collapses have occurred in the study area.

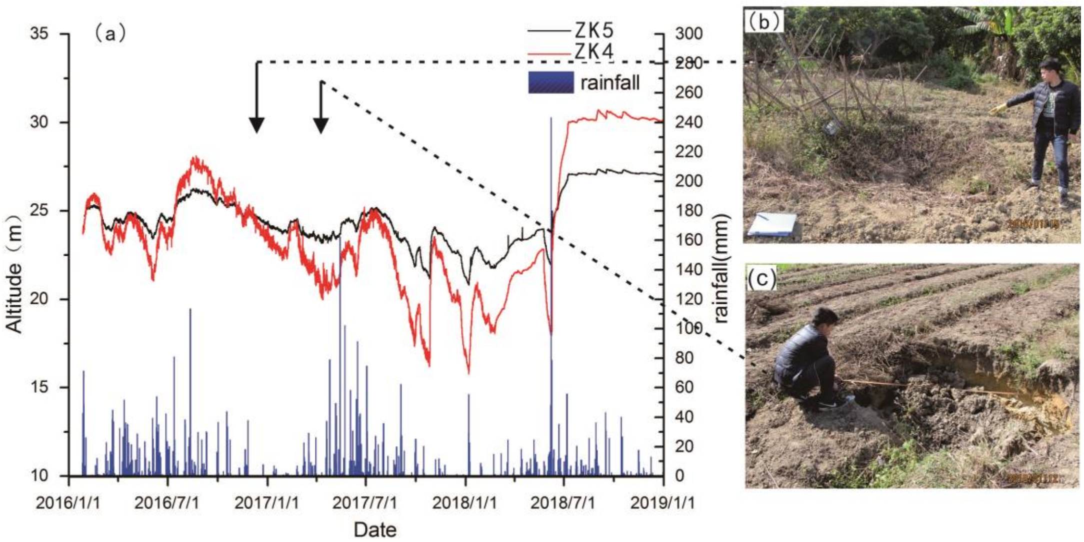

Figure 8. Hydrodynamic monitoring data and cover-collapse sinkholes: (A) Hydrodynamic monitoring data of drilling boreshole ZK5 and drilling borehole ZK4; (B) Image of the cover-collapse sinkhole ID 48; (C) Image of the cover-collapse sinkhole ID 49

4.5 Ground deformations

It was determined in this study that large-sized ground deformations did not exist in the study area, as evidenced by the combined results of the three examined RADARSAT-2 Ultra Fine images taken on November ~~27th of~~ 2015, January ~~14th of~~ 2016, and March ~~2nd of~~ 2016. The InSAR ground deformation data indicated a temporary steady-state in the study area following the occurrences of large-scale ~~sinkhole geological hazards.~~

5. Discussion

In accordance with surveys in China, the analysis processes for cover-collapse sinkhole conditions should involve three main steps, with each step built upon the previous one, as follows:

5.1 Geomorphic analysis

This study illustrated that geomorphic mapping which utilizes historical aerial photographs and unmanned aerial vehicle (UAV) images may be essential for investigations of cover-collapse sinkholes. The UAV images were found to have advantages over the satellite images, due to the fact that they ~~had captured~~ aerial images from certain flying heights with flexible flying missions and time frames. However, the effectiveness of the aforementioned approach may be quite limited in areas where the geomorphic expressions of sinkholes have been obliterated by natural processes or anthropogenic fill. Therefore, on this basis, thorough reconnaissance of the ground would be required to locate sinkholes not identifiable on aerial photographs due to high vegetation cover. It was also determined that information from local residents in the area was conducive to ascertaining the precise spatial distributions of the complex sinkhole clusters, especially concealed sinkholes which may be masked by anthropic landforms. One of the meaningful aspects of this case study was that the geomorphic model produced by combining data from aerial photographs and field surveys could potentially constitute a basis for accurately designing future site investigations and interpreting the results, such as implementing geophysical profiles and borehole data.

5.2 Geological analysis

Due to the complex and ~~sometimes chaotic underlying~~ geology observed in mantle karst areas, investigations which combine several methods are generally the only way to achieve satisfactory geological models for such areas.

Borehole drilling ~~processes~~ are performed in mantle karst regions in order to geotechnically characterize the ~~stratigraphic information~~ and calibrate and validate the geophysical detection results.

However, drilling activities are expensive and time-consuming techniques, and the limited drill footage may potentially have a high degree of uncertainty for the complex underlying geology in karst areas.

However, the punctual information derived from limited numbers of boreholes could be extended laterally using borehole geophysical investigations, such as single-hole radar and cross-hole radar. In this way, other karst caves and fissures ~~around the borehole clouds~~ may be discovered ~~using geological borehole radar techniques~~.

In the present study, based on the limited borehole data, micro-tremor explorations were used to estimate the sediment thicknesses, thereby making it possible to reconstruct the bedrock morphology beneath the entire study area. The non-disturbed areas were represented by the general horizontal bedding of the Quaternary deposits. Therefore, any local thinning or thickening of the Quaternary deposits observed using the mirco-tremor Nakamura technique were believed to indicate the presence of serial sediment within active karst areas.

In addition, the ERI and NSAMT profiles had revealed imaging shallow fault zone structures at the overburden karst area sites. The NSAMT sections were found to have poor measurement effects in the range of 0 to 50 m, and good exploration ~~effects~~ in the range of 50 to 200 m. Meanwhile, the ERI sections had satisfactorily imaged the general geometry of the karst structures in the range ~~of~~ 0 to 50 m. The subsurface cavities and deformation structure clouds were detectable with the GPR, but only up to a limited depth range of 2 to 5 m.

In the present study, the aforementioned techniques were examined in order to determine the most advantageous synergistic approach in the study area. ~~It was expected that the limitations observed in each examined method would be balanced out by the advantages observed in the other methods.~~

5.3 Dynamic monitoring

In order to understand the causes of cover-collapse sinkholes, and to assess and predict the kinematics of the subsidence phenomena, it is generally considered that monitoring methods are necessary. Since karst cover-collapse sinkholes are known to be caused by declines in groundwater levels, a sound knowledge of the short- and long-term dynamics of the ~~effected~~ hydrogeological systems ~~are~~ essential for sinkhole hazard assessments. Hydrodynamic monitoring methods focus on the potential relationships between hydrological changes and the development of cover-collapse sinkholes. The interpretations of the groundwater level monitoring data allow the hydrogeological behaviors of the groundwater to be accurately reconstructed. As a result, the kinematics of the subsidence phenomena can be assessed. In addition, the accurate mapping of ground displacements may serve to identify the locations of future cover-collapse sinkholes and guide future intensive field investigations. Therefore, it was found in this study that monitoring of ground anomalous vertical movements by Interferometric Synthetic Aperture Radar (InSAR) analysis could be an effective approach.

6. Conclusions

(1) In mantle karst regions, cover-collapse sinkholes are considered to be major geohazards due to the large and increasing impacts of sinkhole damages. In this study, based on an appropriate methodological framework, it was found that sinkhole condition analyses were conducive to human security and land-use planning in sinkhole-prone areas.

(2) The multi-disciplinary approach adopted in this study was determined ~~to~~ the most effective method for identifying and understanding cover-collapse sinkhole phenomena in a complex geological frameworks, such as southeastern China’s Bumei Village in the presented case study. The present study’s goal was to contribute to deepening the understanding the genesis and early-stage evolution of a sinkholes

by utilizing geological, geomorphological, and hydrodynamic integrated methodologies. Special focus was paid to the contributions of the various examined methods to overcome ~~the~~ limitations ~~of the other methods.~~

In this case study, a mapping procedure was introduced which combined data from aerial photographs and intensive field investigations. The results clearly indicated the characterization of the cover-collapse sinkholes in the study area. In addition, data interpretations from borehole ~~drilling activities~~ and different geophysical approaches ~~were~~ performed in order to reconstruct the Quaternary deposit features, rock head morphology, and karst features. These examples also indicated why multi-disciplinary and complementary data acquisition approaches were necessary in order to ensure accurrate interpretations in mantled karst settings. For this reason, due to the results obtained in this study, the adopted methodological approach could successfully be extended to other areas characterized by similar geological and hydrogeological characteristics.

(3) In the study village area, the integration of borehole, geophysical, and hydrogeological data suggested that aquifer pumping ~~had~~ triggered the loss of hydrostatic support and accelerated the washing-out processes. As a result, cover sagging and suffosion sinkholes had been generated in the mantled karst region. Although the groundwater levels had been restored at the time of this study, the sinkholes had the potential to again impact the local residents. Therefore, efforts to investigate and monitor the sinkhole development processes in the region will be required to continue into the immediate future.

Acknowledgments

This work was funded by the National Science Foundation(Nos. 41402284, 41472298, 41302255; No. 2018GXNSFAA294020), and the Project of the China Geological Survey (No. DD20160254&

DD20190266).

Reference

Ahmed, S., Carpenter, P.J., 2003. Geophysical response of filled sinkholes, soil pipes and associated bedrock fractures in thinly mantled karst, east-central Illinois. Environmental Geology 44, 705-716.

Al-Halbouni, D., Holohan, E.P., Saberi, L., Alrshdan, H., Sawarieh, A., Closson, D., Walter, T.R., Dahm, T., 2017. Sinkholes, subsidence and subrosion on the eastern shore of the Dead Sea as revealed by a close-range photogrammetric survey. Geomorphology 285, 305-324.

Anchuela, O., Pocoví Juan, A., Soriano, M.A., Casas-Sainz, A., 2009. Characterization of karst hazards from the perspective of the doline triangle using GPR — Examples from Central Ebro Basin (Spain). Engineering Geology 108, 225-236.

Anikeev, A., 1999. Casual hydrofracturing theory and its application for sinkhole development prediction in the area of Novovoronezh Nuclear Power House-2 (NV NPH-2), Russia, Hydrogeology and engineering geology of sinkholes and karst: 1999, pp. 77-83.

Bachrach, R., Mukerji, T., Butler, D., 2005. Analysis of 3D high-resolution shallow seismic and crosswell GPR tomography for aquifer characterization: A case study. Investigations in Geophysics, Near Surface Geophysics: SEG 13, 607-619.

Chalikakis, K., Plagnes, V., Guerin, R., Valois, R., Bosch, F.P., 2011. Contribution of geophysical methods to karst-system exploration: an overview. Hydrogeology Journal 19, 1169.

Chiabrando, F., Nex, F., Piatti, D., Rinaudo, F., 2011. UAV and RPV systems for photogrammetric surveys in archaelogical areas: two tests in the Piedmont region (Italy). Journal of Archaeological Science 38, 697-710.

Cordua, K.S., Nielsen, L., Looms, M.C., Hansen, T.M., Binley, A., 2009. Quantifying the influence of static-like errors in least-squares-based inversion and sequential simulation of cross-borehole ground penetrating radar data. Journal of Applied Geophysics 68, 71-84.

Cueto, M., Olona, J., Fernandez-Viejo, G., Pando, L., López-Fernández, C., 2018. Karst-induced sinkhole detection using an integrated geophysical survey: A case study along the Riyadh Metro Line 3 (Saudi Arabia). Near Surface Geophysics 16, 270-281.

Debeglia, N., Bitri, A., Thierry, P., 2006. Karst investigations using microgravity and MASW; Application to Orléans, France. Near Surface Geophysics 4, 215-225.

Dinesh, B.V., Nair, G.J., Prasad, A.G.V., Nakkeeran, P.V., Radhakrishna, M.C., 2010. Estimation of sedimentary layer shear wave velocity using micro-tremor H/V ratio measurements for Bangalore city. Soil Dynamics and Earthquake Engineering 30, 1377-1382.

Eppelbaum, L., Ezersky, M., Al-Zoubi, A., Goldshmidt, V., Legchenko, A., 2008. Study of the factors affecting the karst volume assessment in the Dead Sea sinkhole problem using microgravity field analysis and 3-D modeling. Advances in Geosciences 19, 97.

Fabregat, I., Gutiérrez, F., Roqué, C., Comas, X., Zarroca, M., Carbonel, D., Guerrero, J., Linares, R., 2017. Reconstructing the internal structure and long-term evolution of hazardous sinkholes combining trenching, electrical resistivity imaging (ERI) and ground penetrating radar (GPR). Geomorphology 285, 287-304.

Frumkin, A., Ezersky, M., Al-Zoubi, A., Akkawi, E., Abueladas, A.-R., 2011. The Dead Sea sinkhole hazard: Geophysical assessment of salt dissolution and collapse. Geomorphology 134, 102-117.

Galve, J.P., Castañeda, C., Gutiérrez, F., Herrera, G., 2015. Assessing sinkhole activity in the Ebro Valley mantled evaporite karst using advanced DInSAR. Geomorphology 229, 30-44.

Gutiérrez, F., Cooper, A.H., Johnson, K.S., 2007. Identification, prediction, and mitigation of sinkhole hazards in evaporite karst areas. Environmental Geology 53, 1007-1022.

Gutiérrez, F., Fabregat, I., Roqué, C., Carbonel, D., Zarroca, M., Linares, R., Yechieli, Y., García-Arnay, Á., Sevil, J., 2019. Sinkholes in hypogene versus epigene karst systems, illustrated with the hypogene gypsum karst of the Sant Miquel de Campmajor Valley, NE Spain. Geomorphology 328, 57-78.

Gutiérrez, F., Galve, J., Lucha, P., Bonachea, J., Jordá, L., Jordá, R., 2009. Investigation of a large collapse sinkhole affecting a multi-storey building by means of geophysics and the trenching technique (Zaragoza city, NE Spain). Environmental Geology 58, 1107-1122.

Intrieri, E., Gigli, G., Nocentini, M., Lombardi, L., Mugnai, F., Fidolini, F., Casagli, N., 2015. Sinkhole monitoring and early warning: An experimental and successful GB-InSAR application. Geomorphology 241, 304-314.

Jiang, X., Lei, M., Zhao, H., 2019. Review of the advanced monitoring technology of groundwater–air pressure (enclosed potentiometric) for karst collapse studies. Environmental Earth Sciences 78, 701.

Kaufmann, G., Romanov, D., Tippelt, T., Vienken, T., Werban, U., Dietrich, P., Mai, F., Börner, F., 2018. Mapping and modelling of collapse sinkholes in soluble rock: The Münsterdorf site, northern Germany. Journal of Applied Geophysics 154, 64-80.

Kim, J.-H., Park, S.-G., Yi, M.-J., Son, J.-S., Cho, S.-J., 2007. Borehole radar investigations for locating ice ring formed by cryogenic condition in an underground cavern. Journal of Applied Geophysics 62, 204-214.

Lee, E.J., Shin, S.Y., Ko, B.C., Chang, C., 2016. Early sinkhole detection using a drone-based thermal camera and image processing. Infrared Physics & Technology 78, 223-232.

Lei, M., Gao, Y., Jiang, X., Guan, Z., 2016. Mechanism analysis of sinkhole formation at Maohe village, Liuzhou city, Guangxi province, China. Environmental Earth Sciences 75, 542.

Lei, M., Gao, Y., Li, Y., Meng, Y., Yu, L., Gan, F., 2008. Detection and treatment of sinkholes and subsurface voids along Guilin-Yangshuo highway, Guangxi, China, Sinkholes and the Engineering and Environmental Impacts of Karst, pp. 632-639.

Maresca, R., Berrino, G., 2016. Investigation of the buried structure of the Volturara Irpina Basin (southern Italy) by microtremor and gravimetric data. Journal of applied geophysics 128, 96-109.

Meng, Y., Ji, F., Jia, L., Jiang, X.-z., Lei, M.-t., 2014. A new approach for forecasting the appearance of sinkholes near the Jinshazhou tunnel. Environmental earth sciences 71, 3339-3347.

Paine, J.G., Buckley, S.M., Collins, E.W., Wilson, C.R., 2012. Assessing Collapse Risk in Evaporite Sinkhole-prone Areas Using Microgravimetry and Radar InterferometryAssessing Sinkhole Collapse Risk Using Microgravimetry And Radar Interferometry. Journal of Environmental and Engineering Geophysics 17, 75-87.

Pueyo Anchuela, Ó., Casas Sainz, A.M., Pocoví Juan, A., Gil Garbí, H., 2015. Assessing karst hazards in urbanized areas. Case study and methodological considerations in the mantle karst from Zaragoza city (NE Spain). Engineering Geology 184, 29-42.

Ronen, A., Ezersky, M., Beck, A., Gatenio, B., Simhayov, R.B., 2019. Use of GPR method for prediction of sinkholes formation along the Dead Sea Shores, Israel. Geomorphology 328, 28-43.

Tan, H., Huang, J., Qi, S., 2012. Application of cross-hole radar tomograph in karst Area. Environmental earth sciences 66, 355-362.

Tharp, T.M., 1999. Mechanics of upward propagation of cover-collapse sinkholes. Engineering Geology, 23-33.

Tharp, T.M., 2002. Poroelastic analysis of cover-collapse sinkhole formation by piezometric surface drawdown. Environmental Geology, 447-456.

Wadas, S.H., Tanner, D.C., Polom, U., Krawczyk, C.M., 2017. Structural analysis of S-wave seismics around an

urban sinkhole: evidence of enhanced dissolution in a strike-slip fault zone. Natural Hazards and Earth System Sciences 17, 2335.
Xeidakis, G., Torok, A., Skias, S., Kleb, B., 2004. Engineering geological problems associated with karst terrains: their investigation. monitoring, and mitigation and design of engineering structures on karst terrains. Bulletin of the geological Society of Greece 36, 1932-1941.
Yeh, M.L., Chou, Y.T., Yang, L.S., 2016. The Evaluation of GPS techniques for UAV-based Photogrammetry in Urban Area. ISPRS - International Archives of the Photogrammetry, Remote Sensing and Spatial Information Sciences XLI-B1, 1079-1084.
Zhou, W., Lei, M., 2017. Conceptual site models for sinkhole formation and remediation. Environmental earth sciences 76, 818.
Zini, L., Calligaris, C., Forte, E., Petronio, L., Zavagno, E., Boccali, C., Cucchi, F., 2015. A multidisciplinary approach in sinkhole analysis: The Quinis village case study (NE-Italy). Engineering geology 197, 132-144.